Second United Nations
International Conference
on the Peaceful Uses of
Atomic Energy

A/CONF.15/P/1026
U.S.A.
June 1958

ORIGINAL: ENGLISH

THE FREE ANTINEUTRINO ABSORPTION CROSS SECTION

DISCLAIMER

DISCLAIMER

Portions of this document may be illegible in electronic image products. Images are produced from the best available original document.

PART I

MEASUREMENT OF THE FREE ANTINEUTRINO ABSORPTION CROSS SECTION BY PROTONS

F. Reines and C. L. Cowan, Jr.*

I. INTRODUCTION

A determination of the cross section for the reaction: antineutrino (ν_-) on a proton (p^+) to yield a positron (β^+) and a neutron (n^o)

$$\nu_- + p^+ \rightarrow \beta^+ + n^o \qquad (1)$$

enables a check to be made on the combination of fundamental parameters on which the cross section depends. Implicit in a theoretical prediction of the cross section are:

1. The principle of microscopic reversibility,
2. The spin of the ν_-,

Los Alamos Scientific Laboratory, University of California, Los Alamos, New Mexico.

* John Simon Guggenheim Fellow, 1957-58; now at the Department of Physics, George Washington University, Washington, D. C.

3. The particular neutrino theory employed: e.g. 2 or 4 component,
4. The neutron half-life and its decay electron spectrum,
5. The spectrum of the incident ν_-'s.

An experiment to identify antineutrinos from a fission reactor[1] was performed which yielded an approximate value for this cross section. Following this work, however (and prior to the parity developments involved in point 3) the equipment was modified in order to obtain a better value of the cross section. The modification consisted in the addition of a cadmium salt of 2-ethylhexanoic acid to the scintillator solution[2] of one of the detectors of reference 1, utilizing the protons of the solution as targets for anti-neutrinos, and making the necessary changes in circuitry to observe both positrons and neutron and neutron captures in the detector resulting from anti-neutrino induced beta decay in the detector. In addition, a second detector used in the experiment of reference 1 was now used as an anticoincidence shield against cosmic-ray induced backgrounds and static shielding was increased by provision of a water tank about 12-inches thick below the target detector. The delayed coincidence count rate resulting from the positron pulse followed by the capture of the neutron was observed as a function of reactor power, and an analysis of the reactor associated signal yielded, in addition to an independent identification of the free antineutrino, a measure of the cross section for the reaction and a spectrum of first pulse (or ν_-) energies. Since the antineutrino spectrum is simply related to the β^+ spectrum the measurement yields an antineutrino spectrum above the 1.8 Mev reaction threshold. The spectrum is, however, seriously degraded by edge effects in the detector.

This experiment is identical in principle with that performed at Hanford in 1953.[3] It was, however, definitive from the point of view of antineutrino identification (whereas the Hanford experiment was not) due to a series of technical improvements coupled with the better shielding against cosmic rays achieved by going underground. The improvements consisted in the use of an isolated power supply to diminish electrical noise from nearby machinery, better shielding from the reactor gamma ray and neutron background, a more complete anticoincidence shield against charged cosmic rays through the use of a liquid scintillation detector, and use of a large detector containing 6.5 times as many proton targets.[4] In addition, oscilloscopic presentation and photographic recording of the data assisted materially in analyzing the signals and rejecting electrical noise.

II. THE EXPERIMENT

Figure 1 represents schematically the sequence of events which occur when an antineutrino is captured by a proton. The cross section $\bar{\sigma}$ for the process for an average fission ν_- is determined from the relationship

$$\bar{\sigma} = \frac{R}{3600\ fn\ \epsilon_{\beta^+}\ \epsilon_{n^o}} \quad (cm^2) \qquad (2)$$

where: R is the observed signal rate in counts/hr,
$n = 8.3 \times 10^{28}$ is the number of target protons,
$f = 1.3 \times 10^{13}$ ν_-/cm^2 sec is the antineutrino flux of the detector, assuming N = 6.1 ν_-/fission,
ϵ_{β^+} is the positron detection efficiency, and
$\epsilon_n{}^o$ is the neutron detection efficiency.

Note that the mean cross section per fission, $\bar{\sigma}$ N, is independent of the number of antineutrinos assumed emitted by the fission-fragments per fission, N.

Uncertainties in the ν_- flux f (5 - 10%) arise from imprecise knowledge of reactor power, uncertainty concerning energy released per fission and the number of ν_- per fission, and incomplete knowledge of the fission fragment distribution in the reactor. The ν_- energy spectrum is determined from a measured β^+ spectrum (or the first-pulse spectrum of the antineutrino produced delayed-coincidences after appropriate energy resolution corrections). The energy E_{ν_-} of the ν_- is related to $E_{\beta+}$, the kinetic energy of the product β^+, by the equation

$$E_{\nu_-} = 3.53 + E_{\beta+} \quad (mc^2 \text{ units}) \tag{3}$$

We have neglected the few kilovolt recoil energy of the product neutron.

With these quantities in mind we will describe the experiment in conjunction with a schematic diagram of the equipment, Fig. 2.[5] Assume that an antineutrino induced reaction occurs in the detector. The β^+ signal is seen by each of two interleaved banks of 55, 5-inch Dumont photomultiplier tubes in prompt coincidence within the 0.2 μsec resolving time of the equipment. The signals are added by preamplifiers whose gains have been balanced to allow for slight differences in the response of the two photomultiplier banks, amplified further and sent via a 30 μsec delay-line to the deflection plates of a recording oscilloscope. At the same time the two signals are sent separately to a prompt coincidence unit (marked β^+) which accepts them if they correspond to pulse height amplitudes between 1.5 and 8 Mev. On receipt of an acceptable signal, the β^+ scaler is tripped, and a gating pulse is sent to the second coincidence unit (marked n). If during a prescribed time (3/4 → 25-3/4 μsec) following the β^+ pulse, a neutron pulse corresponding to an energy deposition of 3 to 10 Mev in the antineutrino detector occurs (again in prompt coincidence from the two interleaved photomultiplier banks) the neutron coincidence unit signals a delayed coincidence. This delayed coincidence is registered by a scaler and triggers the scope sweep, allowing the entire sequence which has been stored in the 30 μsec delay lines to be displayed and photographed. The neutron prompt coincidences are also recorded by a scaler.[6] Therefore, the raw data obtained for analysis are the following: the rates in the positron and neutron gates; delayed coincidence rate, scope trigger rate, pulse amplitudes and time intervals between pulses as seen on the recording oscilloscope. These data are obtained with the reactor on and off and with gross changes in bulk shielding.

In addition to the above arrangement there is provision for the reduction of cosmic ray associated background by means of an anticoincidence detector placed above the antineutrino detector as shown in Fig. 2. If, for example, a pulse occurs in the anticoincidence detector of amplitude > 0.5 Mev in coincidence with otherwise acceptable β^+-like pulses, the event is not accepted by the β^+ coincidence-anticoincidence unit and hence is not recorded by the oscilloscope. This is a reasonable criterion since the annihilation radiation which might reach the anticoincidence detector for a bonafide ν_- event is at most 0.5 Mev. In order to reduce the background from events secondary to the passage of high energy (> 8 Mev) charged cosmic rays and delayed in time, the β^+ coincidence unit had incorporated into it a long upper gate which rendered the system insensitive for 60 μsec following such a pulse. Pulses triggered by electrical noise are also eliminated by means of the distinctive visual record.

IIa. CALIBRATIONS

Calibrations of energy and time-interval response were made periodically. The first was accomplished by employing the μ-meson "through-peak" energy, the second by means of standard time markers put directly on the oscilloscope traces from a crystal oscillator. Gate lengths were checked against a time delay calibrator designed for the purpose. Fig. 3 shows the through-peak, a pulse-amplitude distribution resulting from the vertical passage through the tank of penetrating cosmic ray μ-mesons, taken before and after the present experiment for each of the two interleaved photomultiplier tube banks. Since most of the mesons are minimally ionizing, and the depth of the liquid is 60 cm, the specific energy loss[7] in the liquid of 1.57 Mev/cm gives the location of the peak as 100 Mev. The peak represents a slightly higher energy than that calculated from the energy loss/cm times the tank depth because of the finite lateral extent of the tank and the angular distribution of the cosmic rays. The peak is located to an accuracy of ± 5%. Since the detector response is proprotional to the energy deposited in it, a standard linear pulser was calibrated with the through-peak amplitude and then used to calibrate the system in turn and set the appropriate gates. Based on measurements using artificial radioactive sources and the μ-meson decay electron spectrum end point in our large liquid scintillation detectors, the error in energy calibration is believed to be less than ± 10%.

IIb. DETERMINATION OF THE SIGNAL RATE, R

The signal rate R was determined from the four series of measurements summarized in Table I. In principle the procedure is straightforward: the accidental background rate $A(hr^{-1})$ is determined for each run from the relation

$$A = 3600\, \alpha\, \bar{n}\, \bar{\beta}^+\, \tau \qquad (hr^{-1}) \qquad (4)$$

where: $\tau = 25 \times 10^{-6}$ sec, delayed coincidence gate length,
$\bar{n}$ and $\bar{\beta}^+$ are the rates averaged over each run as measured by the scalers, and
α = overlap factor for counts in n and β^+ gates.

We see from a comparison of the delayed coincidence rate as given by the scalers and film analysis, however, that about 1/3 of the scaler rate is rejected as unsuitable on inspection of the film traces. This means that the accidental background rate calculated for the record n and β^+ scalers is too high by a factor of about 1/3. In addition, since the energies in the n and β^+ gates overlap, and judging by the rates in these gates, $1.23 > \alpha > 1.00$. Basing our calculations on the scope films, we find the net rates (total less accidental) for the four categories of runs which we list in Table II. Since $\alpha < 1.23$ and the truth is between ⓐ and ⓒ, we quote $R = 36 \pm 4\ hr^{-1}$, where ± 4 includes the statistical error listed in column ⓐ and an allowance for the drift in the energy calibration, which analysis of the data shows likely to have occurred in the period between the series of runs A and C. The ratio of the $\bar{n}/\bar{\beta}^+$ rates is lower for runs C than for A. This is consistent with an increase in the overall gain of the system, since the background spectrum decreases monotonically with increasing energy, and an increase in gain would bring in relatively more lower energy pulses. Runs D were made to demonstrate that the sawdust shield, though effective in reducing neutron signals from an Am-Be source (and hence reactor neutrons) by a factor of 15 and gammas by a factor of 2, had no effect on the anti-neutrino signal. The antineutrino flux during D was up by 10% because of a change in reactor power which happened to coincide with these runs. When corrected for this rise in reactor power the results from D are consistent with the other runs.

IIc. SIGNAL/BACKGROUND

From Tables I and II we conclude that the signal to total background ratio is approximately 1/5 with the background about equally divided between correlated and accidental events. Correlated events arise primarily from fast neutrons produced by μ-meson capture in the vicinity of the detector: the first pulse is produced as a proton recoil, the second by the capture of the neutron in the scintillator cadmium. The correlated reactor associated background is deduced from the absence of an observable effect due to the 75 cm sawdust shield (density 0.5 gm/cm^3, neutron shielding factor; 15) to be $<1/10$ the signal. An accidental background increase of 15 hr^{-1} was associated with the reactor so that the signal to accidental reactor-associated background ratio was about 2/1.

IId. EFFICIENCY ESTIMATES

In order to evaluate the cross section, we require the efficiencies ϵ_{β^+} and ϵ_n. Since these quantities were inferred rather than measured directly, some discussion of the efficiency evaluation procedure employed is in order.

ϵ_{β^+}

It is evident that the β^+ detection efficiency is high because of the small probability of β^+ leakage from the detector. The problem is to determine with what probability the event fell within the energy gates employed, i.e. $1.5 \rightarrow 8$ Mev. To estimate this probability, plots were made of the first pulse spectrum

with the reactor on and off as measured in runs A, B, C. Figure 4 shows the spectrum of first pulses scaled to run time of 47.3 hrs. The lowest energy points are seen to drop sharply, a fact attributed to the effect of energy gates cutting into the spectrum. Since the background spectrum should continue to rise with decreasing energy, the reactor on-off difference was scaled up by a factor determined from an extrapolation to lower energies and is shown on the first pulse difference curve on Fig. 5. In deriving the difference curve, no account was taken of the increase in accidental background associated with the reactor, and so the curve rises more sharply at lower energies than does the true β^+ spectrum. The β^+ detection efficiency was deduced from this curve by extrapolating to the origin and measuring the fraction of the area in the experimental vs the extrapolated curve. This procedure underestimates the efficiency somewhat because a subsequent measurement of the ungated spectrum seen from a Cu^{64}, β^+ source dissolved in the scintillator showed no pulses of energy < 0.45 Mev, whereas we have here assumed pulses down to 0 Mev. Accordingly, the β^+ efficiency estimate from Fig. 5, (0.81) is raised slightly and taken to be $\epsilon_{\beta+} = 0.85 \pm 0.05$, where 0.05 is meant to indicate the limits of error in ϵ_{β^+}.

ϵ_n

The neutron detection efficiency is somewhat more difficult to estimate. This efficiency is given as the product of three factors:

$$\epsilon_n = \epsilon_{n_1} \epsilon_{n_2} \epsilon_{n_3} \qquad (5)$$

where: ϵ_{n_1} = probability that the neutron will not leak out of the system,
ϵ_{n_2} = probability that the neutron will be captured in the scintillator cadmium in the 25 μsec time interval (3/4 → 25-3/4 μsec) after its birth.
ϵ_{n_3} = probability that the neutron capture gamma rays will produce a signal which falls within the chosen energy gates, 3 → 10 Mev.

ϵ_{n_1} is estimated from a consideration of the detector volume fraction within an antineutrino produced neutron mean free path of the detector surface. From the conservation laws applied to reaction (1) the neutron energy is $\lesssim$ 10 kev and therefore has a mean free path in the scintillator of about 1 cm. The fraction of the detector volume within 1 cm of the edge is about 6% and approximately 1/2 (or 3%) of the neutrons born in this region will be travelling outward, hence $\epsilon_{n_1} = 0.97$.

ϵ_{n_2} is the least certain of the factors involved in the neutron detection efficiency. It was estimated in two ways: by an interpolation of the curves calculated via the Monte Carlo method for cases[8] involving higher Cd/H ratios than the one used in this experiment (here Cd/H = 0.000145) and by integration of the cadmium capture probability for thermal neutrons from 3/4 → 25-3/4 μsec after their introduction into the scintillator. The interpolation gives $\epsilon_{n_2} = 0.15$ with a ± 0.02 uncertainty. Neglecting capture competition by the scintillator hydrogen the mean time for capture $\tau_{Cd} = 161$ μsec, and the capture probability is calculated to be 0.142. Since the mean capture time in

scintillator hydrogen τ_H = 235 μsec, the hydrogen captures in this period lower the captures in Cd so that ϵ_{n_2} = 0.135.

ϵ_{n_3} is estimated in much the same way as was ϵ_{β^+}. Figure 6 shows the first pulse ^{3}spectra in runs A and B normalized to 47.3 hrs. Fig. 7 shows the difference spectrum and A_1/A_2 = 0.68. Since, as with the first pulse spectrum, no allowance was made for the accidental background, we take

$$\epsilon_{n_3} = 0.75 \pm 0.05$$

where ± 0.05 is meant to indicate the limits of error in ϵ_{n_3}.

Summarizing, ϵ_n = 0.97 x 0.75 x 0.14 = 0.10. It seems reasonable to assign error limits of ± 20% to this efficiency. An experimental attempt to measure the neutron detection efficiency succeeded only in setting a lower limit of 6%. Figs. 8 and 9 show the distribution of time delay intervals between the pairs of pulses comprising the delayed coincidences. The curves are characteristic of neutron captures in the scintillator.[8]

IIe. THE CROSS SECTION

Inserting the efficiency numbers etc. into Eq. (2) we find the cross section for fission antineutrino absorption by protons.

$$\bar{\sigma} = \frac{36 \pm 4}{3600 \times 1.3\times10^{13} \times 8.3\times10^{28} \times (0.85 \pm 0.05) \times (0.10 \pm 0.02)}$$

$$= 11 \pm 4 \times 10^{-44} \text{ cm}^2/\nu_-$$

or,

$$\bar{\sigma}N = 6.7 \pm 2.4 \times 10^{-43} \text{ cm}^2/\text{fission}$$

where the ± is obtained by adding the listed errors and hence is a severe estimate of the uncertainty.

IIf. THE ν_- SPECTRUM FROM FISSION FRAGMENTS

It is possible to deduce the fission fragment ν_- spectrum from a measurement of the β^+ energies in reaction (1) and a knowledge of the cross section for the process. Because of the large experimental error involved in our determination of the β^+ spectra, the resultant ν_- spectrum is very poorly determined. Nonetheless it seems worthwhile to make such a deduction. Apart from statistical fluctuations the major uncertainty is in the energy resolution of the system. This uncertainty is due to leakage of one 0.511 Mev annihilation gamma ray from the detector and the poor energy resolution (± 25%) for

1 Mev deposited in the large detector. The effect of gamma ray leakage on the spectrum was checked by dissolving a Cu^{64}-octoate source in the scintillator and measuring the energy spectrum. It was somewhat distorted, but the main effect was to drop the energy by about 0.5 Mev.

The β^+ spectrum $n(E_{\beta^+})$ and ν_- spectrum $m(E\nu_-)$ are related[9] by the equation

$$m(E\nu_-) = n(E_\beta)\ \sigma(E\nu_-)$$

Fig. 10 shows $m(E\nu_-)$. Gamma ray leakage was considered in that the β^+ curve was shifted to the right by 0.5 Mev prior to the calculation. The data are not considered sufficiently accurate to warrant estimation of the distortion due to the energy resolution of the detector.

III. REMARKS CONCERNING AN IMPROVED MEASUREMENT

At least two major improvements could be made in this measurement to increase the counting rate and improve the energy resolution. The neutron detection efficiency can be raised from its present 10% to about 80% by increasing the cadmium content of the scintillator by a factor of 20. This can be done without unreasonable reduction in the light transmission and scintillator efficiency by using the highly purified cadmium octoate, recently developed by A. R. Ronzio.[10]

In addition, redesign of the detector using an inner "cadmiated" region enclosed in a noncadmium bearing scintillator would minimize end effects due to gamma-ray leakage from the detector. Such an increase in detection efficiency would enable a factor of ten reduction in the size of the antineutrino sensitive (or cadmiated) volume without undue sacrifice in signal rate. At presently available antineutrino fluxes, a signal rate of 30 hr^{-1} or more would result from the smaller improved detector. The signal-to-accidental background ratio would be raised by a factor of about ten for a 25 μsec delayed coincidence gate because of the increase in the signal rate and the decrease in detector size. The uncadmiated scintillator blanket should help shield against cosmic ray correlated events which are due to a neutron produced by μ-meson capture in the vicinity of the detector. A cylindrical shape with photomultiplier tubes placed around the cylinder wall would make for a uniform light collection and hence improved energy resolution. This detector could be shielded against cosmic rays with the anticoincidence detector as before, and much the same electronics could be used.

IV. RESULT

The measured cross section for the absorption by protons of fission fragment antineutrinos is $\bar{\sigma}N = 6.7 \pm 2.4 \times 10^{-43}$ cm^2/fission.

V. ACKNOWLEDGEMENTS

The authors wish to thank Mr. H. W. Kruse for his analysis of the film records. Drs. F. B. Harrison and A. D. McGuire and Messrs. R. Jones and M. P. Warren helped set up the equipment. Many groups in the Los Alamos Laboratory have given support in the design and construction of the equipment. We wish especially to thank the Shops Department under Mr. G. H. Schultz and the Electronics Group under Mr. John Lamb. The hospitality of the E. I. duPont de Nemours Company which operates the Savannah River Plant of the United States Atomic Energy Commission is also gratefully acknowledged.

REFERENCES AND FOOTNOTES

1. Cowan, C. L., Jr., Reines, F., Harrison, F. B., Kruse, H. W., McGuire, A. D., "Detection of the Free Neutrino: a Confirmation", Science, 124, 3212 (1956).

2. The article "Liquid Scintillators for Free Neutrino Detection", by Ronzio, A. R., Cowan, C. L., Jr., and Reines, F., Rev. Sci. Instr. (in press) describes the preparation and handling of liquid scintillators developed for the Los Alamos neutrino program.

3. Reines, F., and Cowan, C. L., Jr., "Detection of the Free Neutrino", Phys. Rev. 90, 492 (1953).

4. The gain, times 6.5, due to the increase in target protons was largely balanced by a decrease in the neutron detection efficiency, times 1/3, made necessary by other experimental considerations.

5. Photographs of the detectors and some associated equipment may be found in "Neutrino Physics", Reines, F., and Cowan, C. L., Jr., Physics Today 10, No. 8, 12 (1957). Detector details are described in an article by Reines, F., in the forthcoming book "Methods of Experimental Physics, Vol. 5", edited by Drs. Yuan, L. C., and Wu, C. S., Academic Press, Inc., New York.

6. To be precise we should use the phrases "β^+ like" and "n like" to describe the pulses because pulses in these energy ranges are produced by other particles as well.

7. This value is obtained from Fig. 2.9.1 of the book by Rossi, B., "High Energy Particles". Prentice-Hall (1952), using a carbon density of 0.88 gm/cm^3.

8. "Detection of Neutrons with a Large Liquid Scintillation Counter", by Reines, F., Cowan, C. L., Jr., Harrison, F. B., Carter, D. S., Rev. Sci. Instr. 25, 1061 (1954).

9. The cross section for monoenergetic ν_- is given in Part II of this paper by Carter, R. E., Reines, F., Wagner, J. J., and Wyman, M. E.

10. Ronzio, A. R. (private communication). Another solution, cadmium propionate in toluene with the suggested Cd/H ratio, = 0.003, was used in the Hanford work[2,8] but its generally undesirable characteristics, e.g. fire hazard and toxicity, militated against its use in the present experiment.

TABLE I

SUMMARY OF RUNS

Run No.	Comments	Run length (hrs)	Scaler Readings			Total Scope Film Accept Rate (hr^{-1}) (in 25 μsec)
			n(sec^{-1})	β^+(sec^{-1})	Del.coinc(hr^{-1}) (25 μsec gate)	
232	Reactor ON, wet	2.05	15.9	68.5	307.8	212.6
233	sawdust shield	14.43	15.8	67.5	304.5	220.3
234	in place.	8.0	15.6	66.6	302.6	209.4
235		13.30	15.6	66.8	297.8	205.3
236	(Category A)	9.5	15.4	67.0	299.5	214.8
237	Reactor OFF,	12.47	14.3	65.0	251.0	165.6
238	sawdust shield	9.37	14.0	63.6	249.0	170.9
240	in place	9.54	14.2	68.0	256.6	173.7
241		14.43	14.5	66.3	251.8	170.1
243	(Category B)	6.77	14.4	65.4	251.1	163.5
246	Reactor ON,	12.20	16.3	71.6	313.4	228.3
247	sawdust shield	2.00	16.2	71.1	300.0	213.5
248	in place.	11.12	16.1	71.1	314.5	224.4
249		9.53	16.2	71.2	327.2	236.6
251	(Category C)	10.53	16.5	72.4	320.9	226.2
252		11.67	16.2	71.5	324.7	232.6
253		8.92	16.3	71.6	316.3	222.5
255	Reactor ON,	6.48	17.2	75.2	334.4	250.5
256	sawdust removed.	10.38	17.3	76.0	331.1	240.2

Note: Runs are listed in chronological sequence. Missing runs were omitted either because they were incomplete or were not a relevant part of this series.

TABLE II

SUMMARY OF RESULTS

Run Category	Net Rate (hr^{-1}) = Gross Rate Less Calculated Accidental Background.			Results
	ⓐ bkd. reduced by signal ratio and $\alpha = 1$	ⓑ no correction for "1/3" factor and $\alpha = 1$	ⓒ correction for "1/3" factor and $\alpha = 1$	Reactor associated signal = $\frac{(C-B)66 + (A-B)47.3}{113.3}$
A (47.3 hrs)	146.2 ± 1.7	118.4	130.8	ⓐ 38 ± 3 (hr^{-1})
B (52.6 hrs)	112.2 ± 1.5	84.4	99.1	ⓑ 37 ± 3
C (66.0 hrs)	153.0 ± 1.4	123.3	135.8	ⓒ 35 ± 3
D (16.9 hrs)	157.9 ± 2	126.6	138.1	

PARTS LIST

Electronics parts list	Model	LASL Drawing Number
Preamplifiers	250	4Y-26448 C-3
Amplifiers	251	4Y-26760
Positive HV Supplies	21	4Y-26794 C
Scalers	720	4Y-26722, 4Y-26062
	750A	4Y-26065 C-8
Coincidence-anticoincidence units	1	4Y-26845 D-2; 4Y-26844 D-2
Recording Oscilloscope	2	4Y-26807
Pulser	506	4Y-26689
Pulse-height Analyzer	103	4Y-26522
Scope Camera Power Supply		33Y-22101, C-1
Time Delay Calibrator	101	4Y-26179
Delay Lines	HH 2000 - RG 176/U	
Scope Camers	35 mm Fairchild Model F-246A	

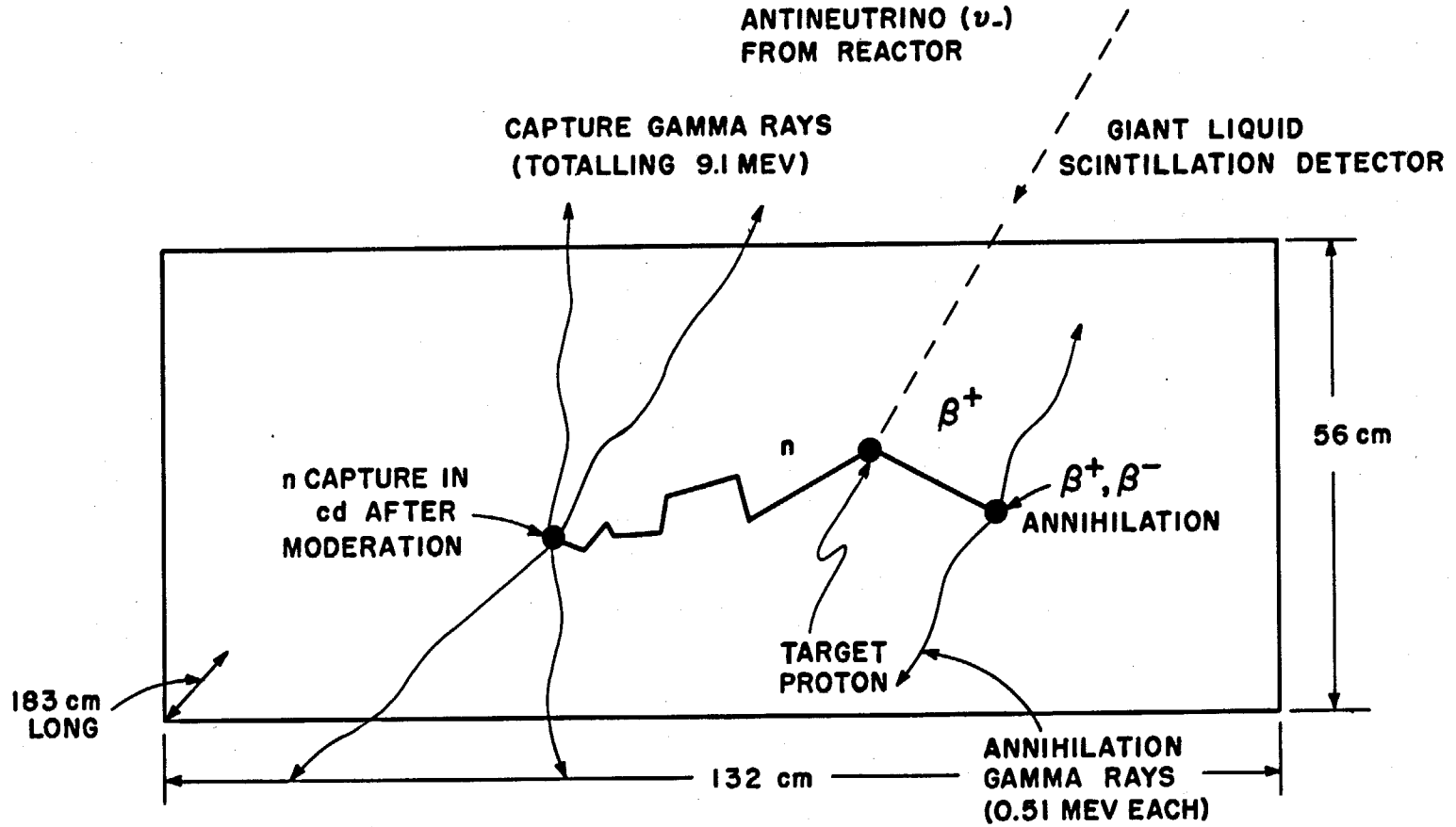

Figure 1

Schematic of Antineutrino Detector. This 1.4×10^3 liter detector is filled with a misture which consists primarily of triethylbenzene (TEB) with small amounts of p-terphenyl (3 gm/liter), POPOP wavelength shifter (0.2 gm/liter) and cadmium (1.8 gm/liter) as cadmium octoate. An antineutrino is shown transmuting a proton producing a neutron and positron. The positron slows down and annihilates, producing annihilation radiation. The neutron is moderated by the hydrogen of the scintillator and is captured by the cadmium, producing capture gamma rays.

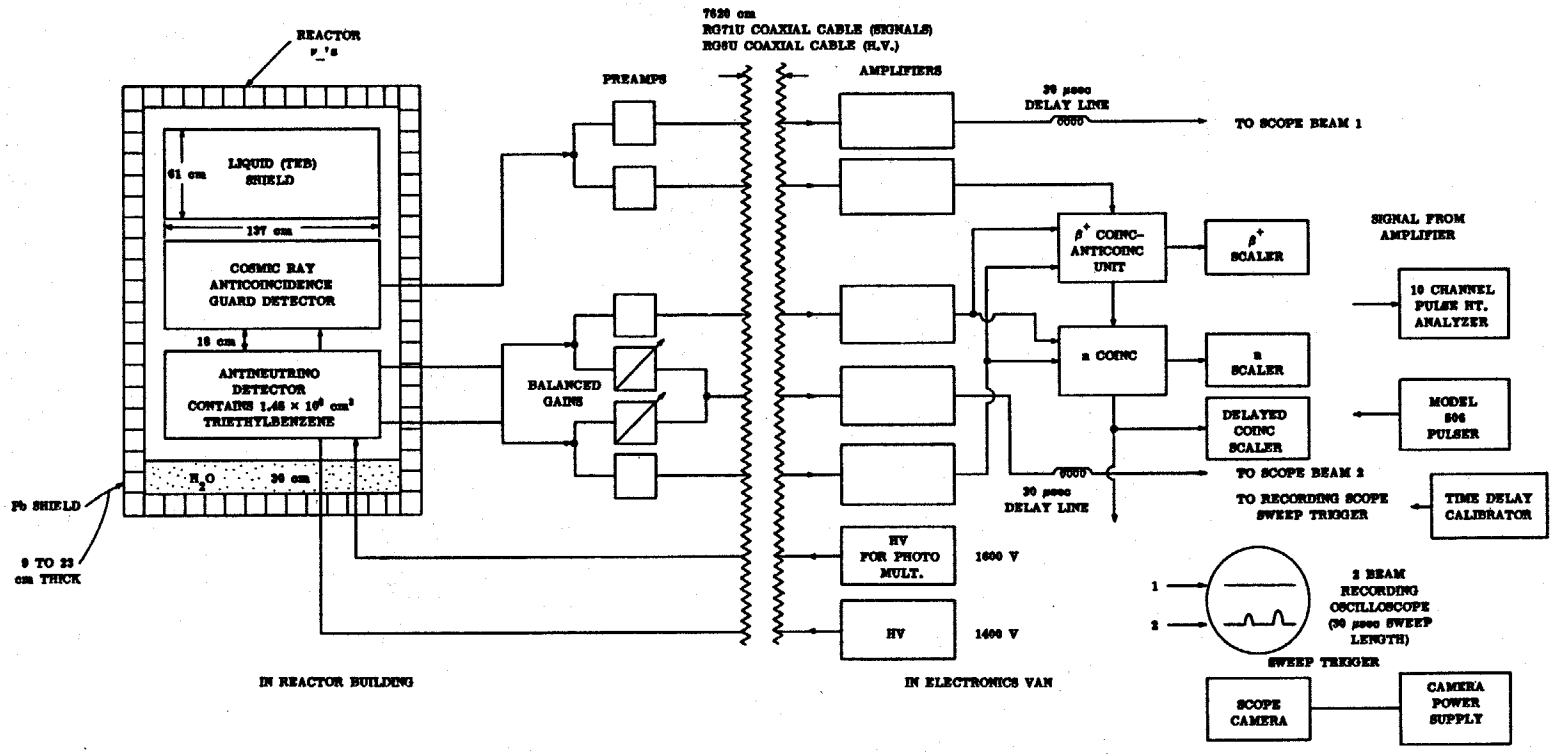

Figure 2

Schematic of Experimental Arrangement.

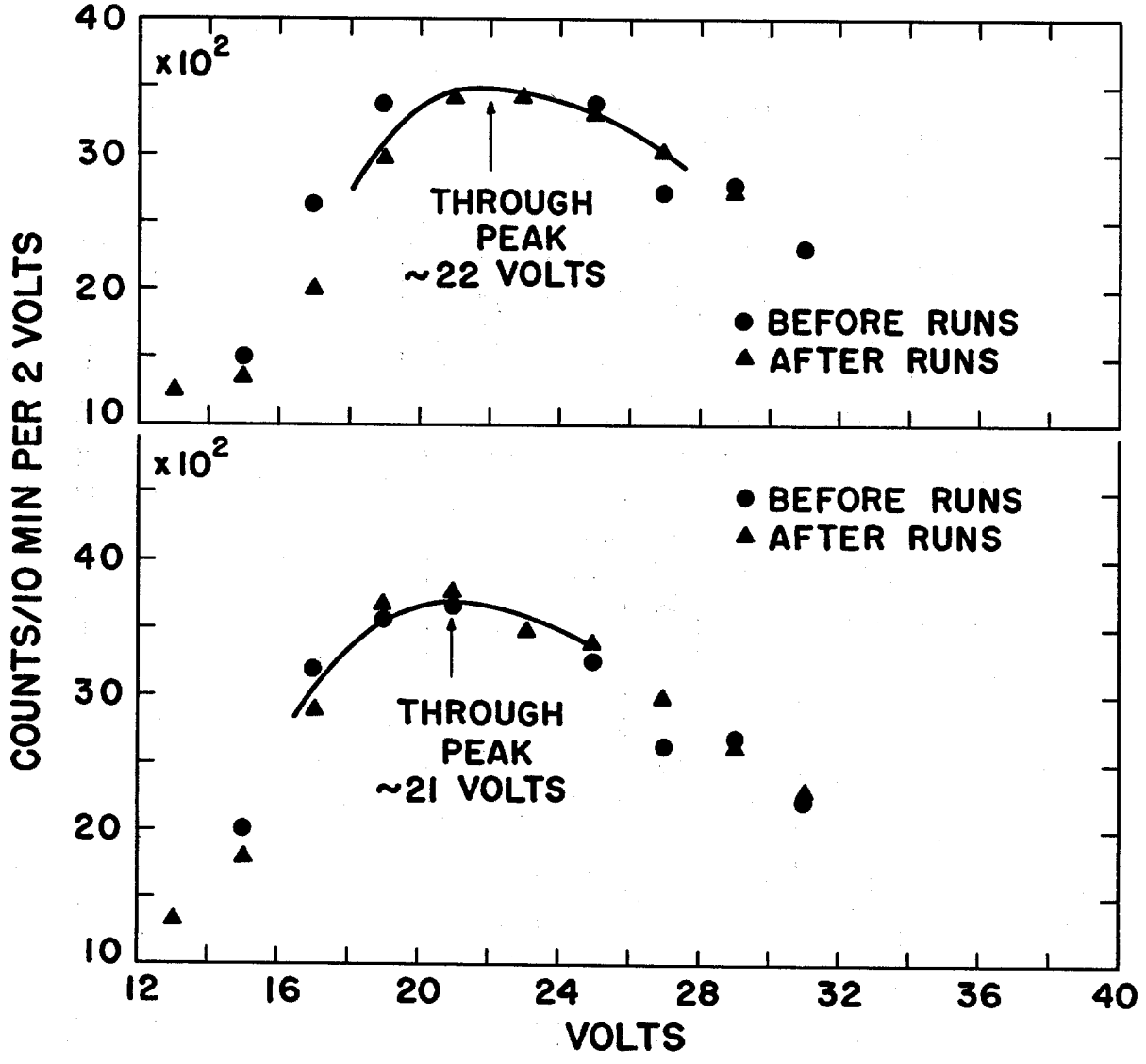

Figure 3

Ungated through meson peaks for energy calibration and stability check.

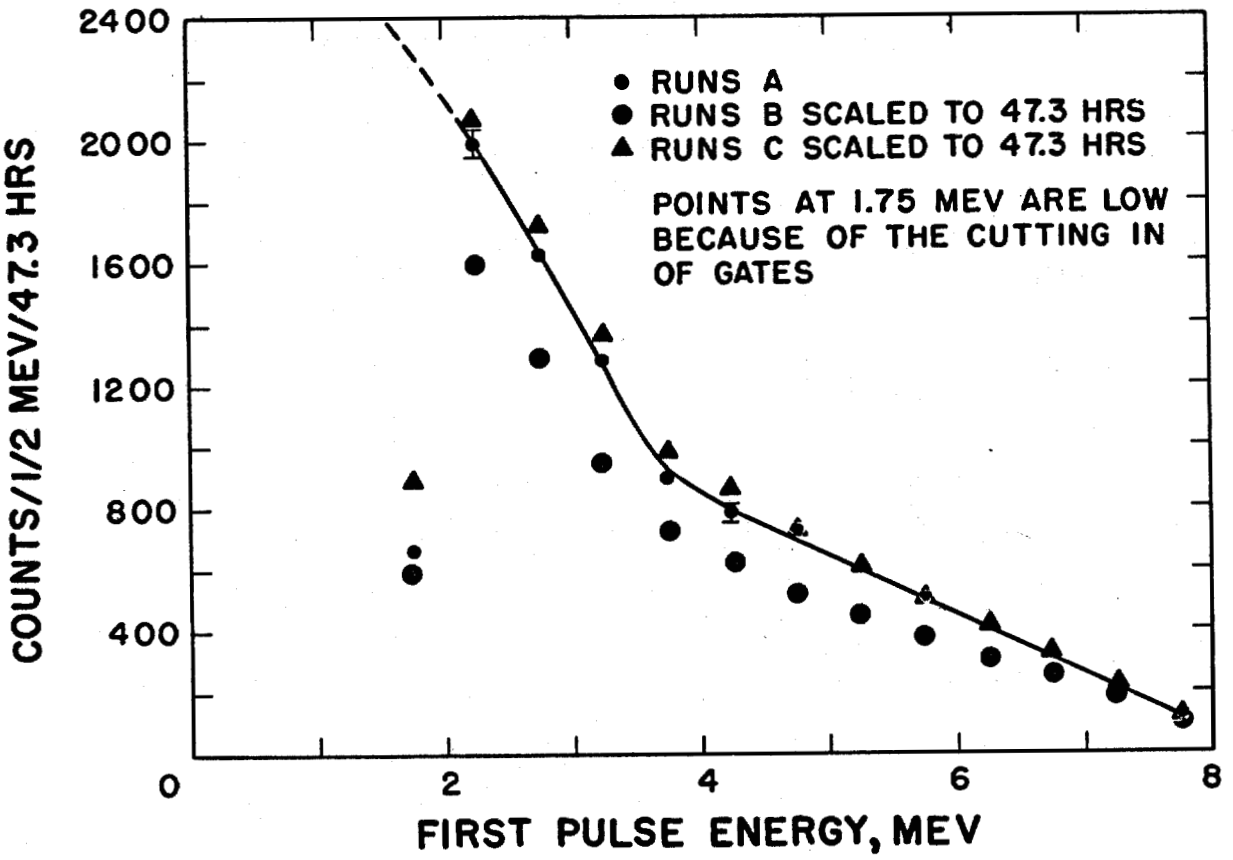

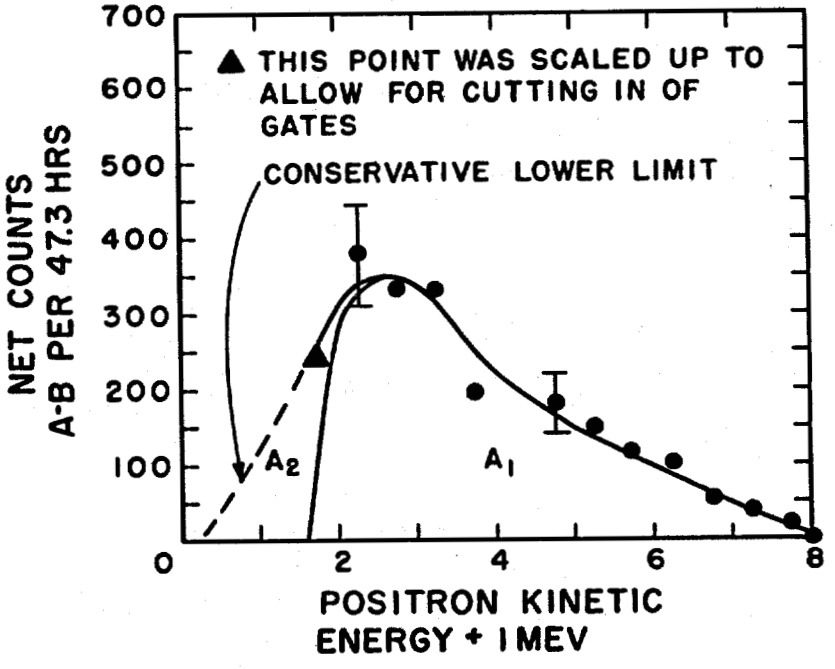

Figure 4. First pulse spectrum.

Figure 5. Positron spectrum, $A_1/(A_1 + A_2) = 0.81$. No correction is made here for reactor associated background. This background raises the lower energy part of the spectrum and hence $\epsilon_{\beta+} > 0.81$. Take $\epsilon_{\beta+} = 0.85 \pm 0.05$.

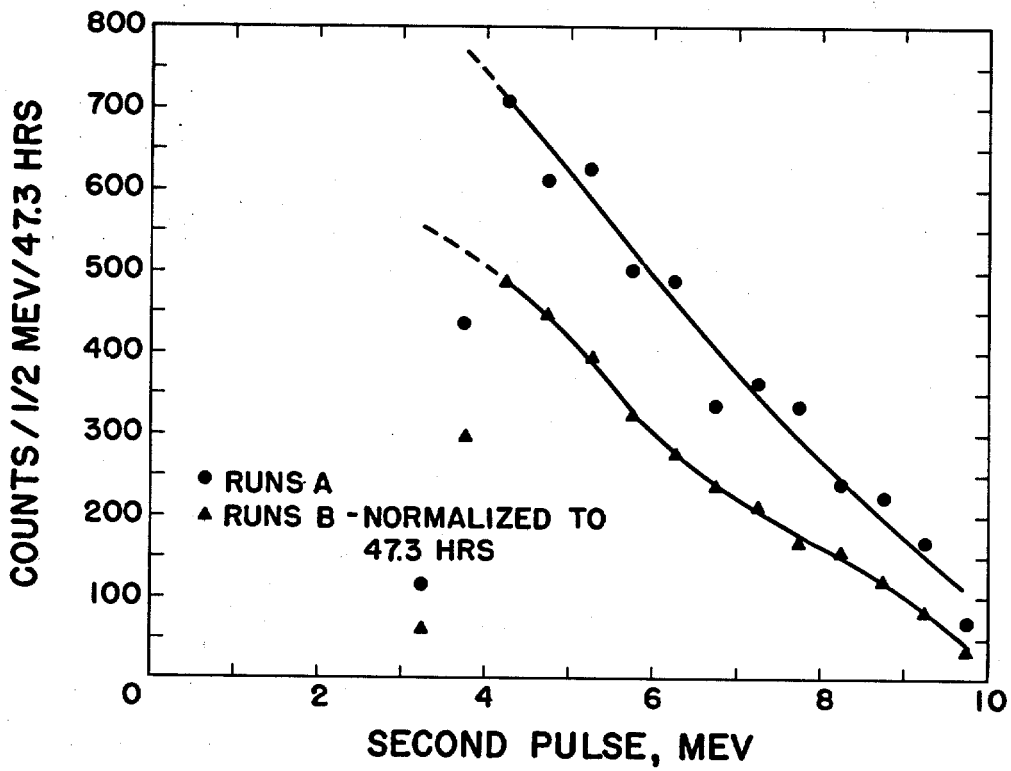

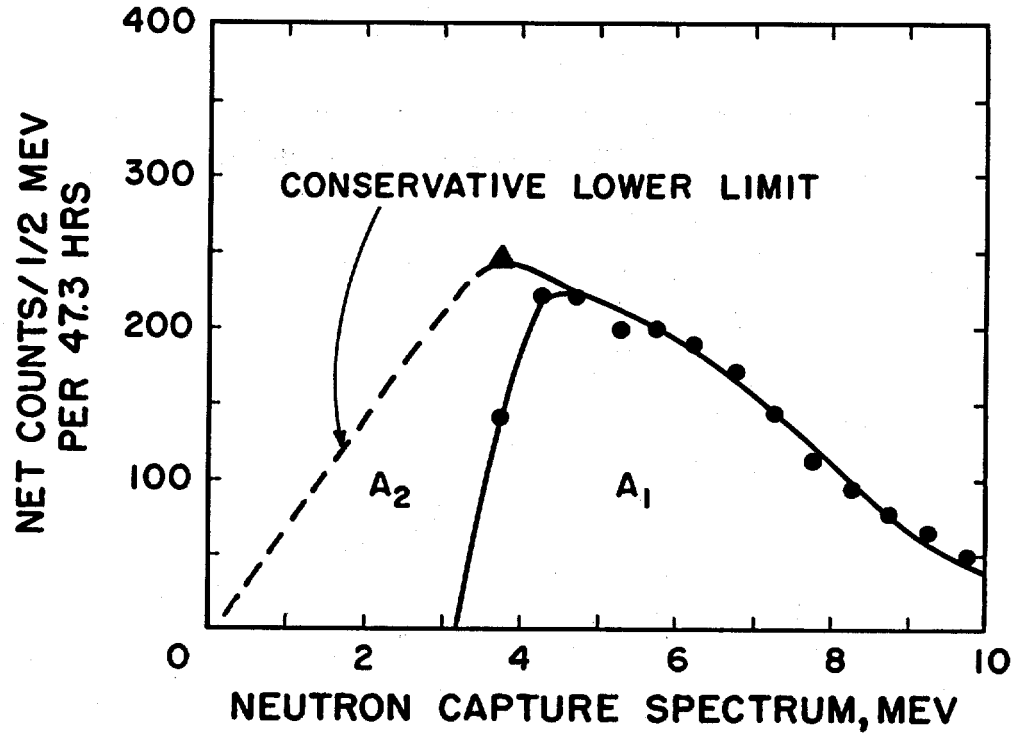

Figure 6. Second pulse spectrum.

Figure 7. Neutron Capture Gamma Spectrum. $A_1(A_1 + A_2) = 0.68$. No correction is made here for reactor associated background. This background raises the lower energy part of the spectrum and hence $\epsilon_{n_3} > 0.68$. Take $\epsilon_{n_3} = 0.75 \pm 0.05$.

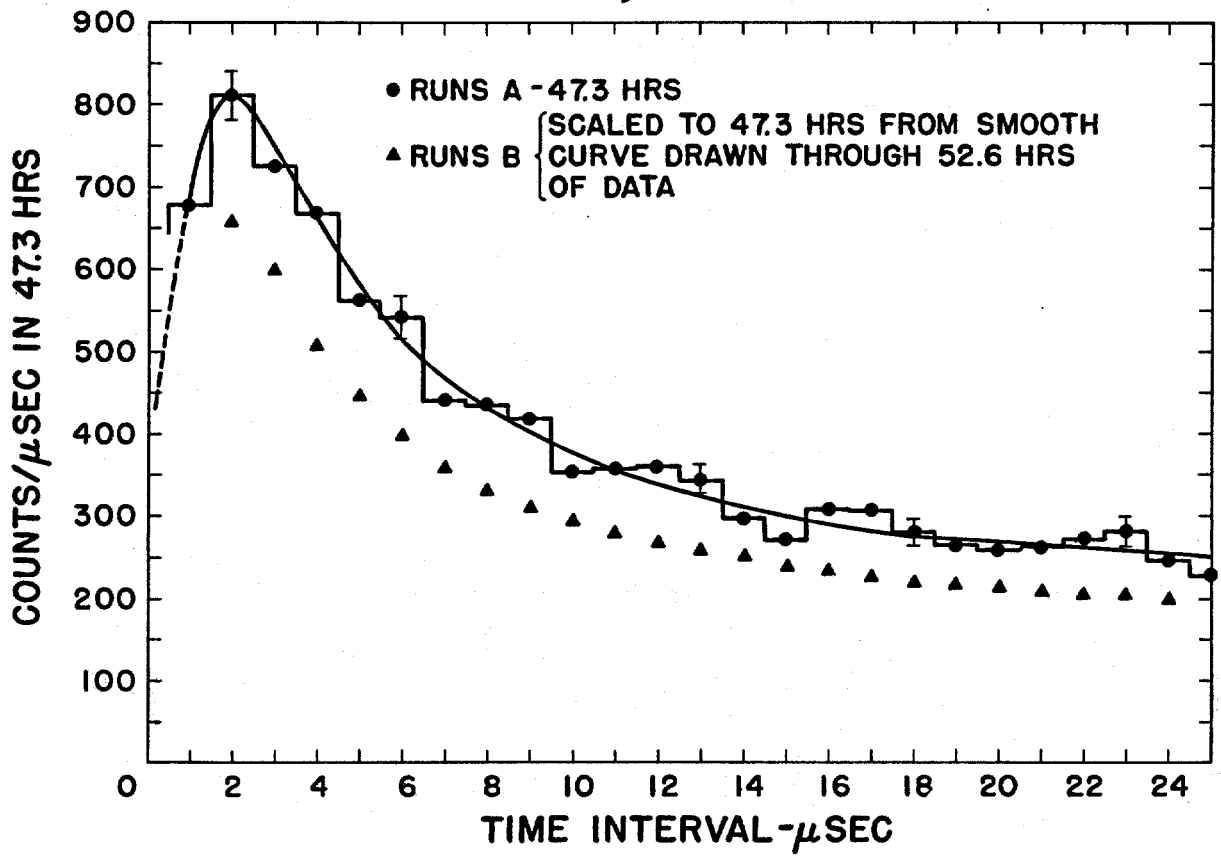

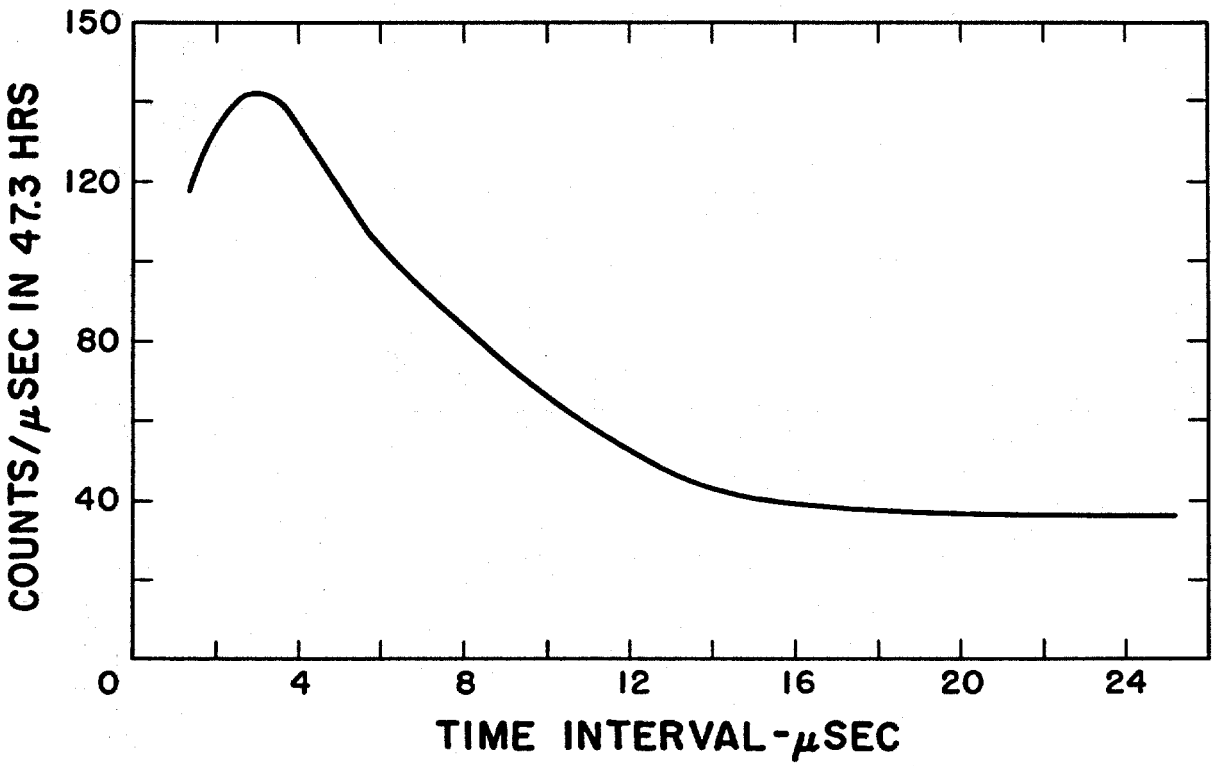

Figure 8 Distribution of time intervals between pulses. Runs A (47.3 hrs) Runs B (Scaled to 47.3 hrs from smooth curve drawn through 52.6 hr of data.)

Figure 9 Reactor associated distribution of time intervals between pulses Runs A-B (Normalized to 47.3 hrs).

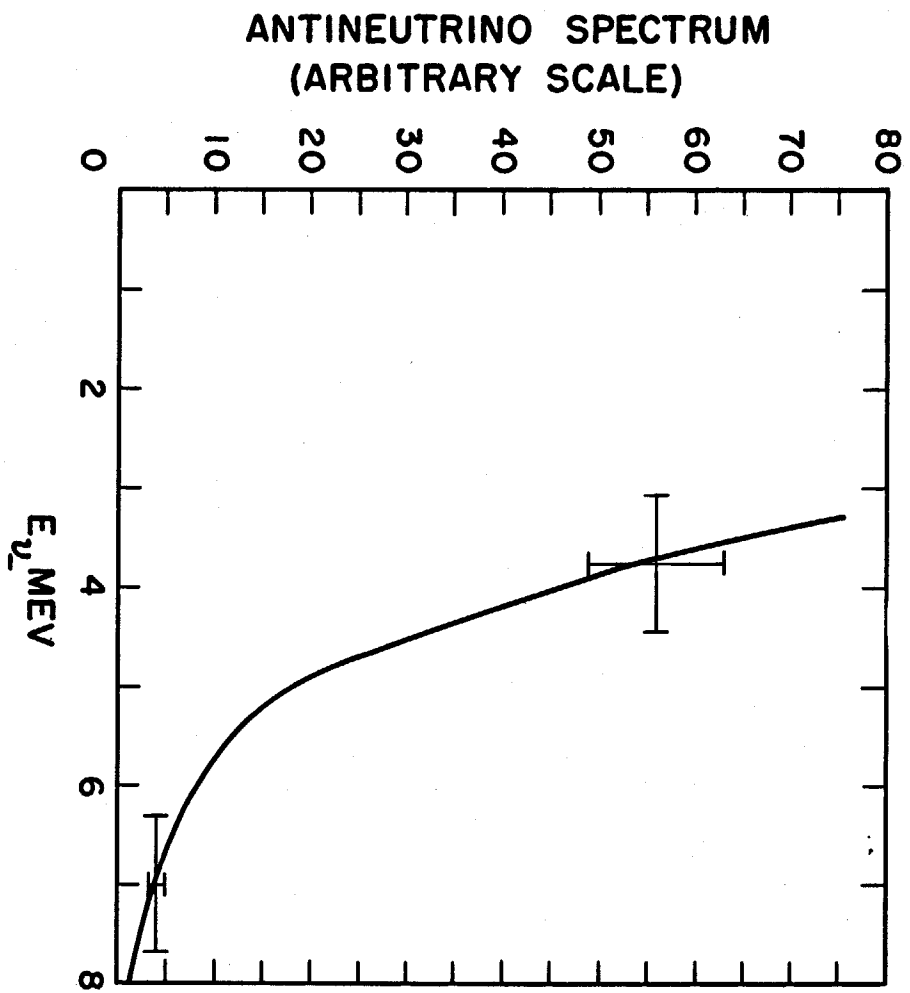

Figure 10

Antineutrino spectrum from fission fragments deduced from β^+ spectrum in reaction $\nu_-(p^+,n^o)\beta^+$. Crosses ⊢ denote estimates of uncertainties.

PART II

EXPECTED CROSS SECTION FROM MEASUREMENTS OF FISSION FRAGMENT ELECTRON SPECTRUM

R. E. Carter, F. Reines, J. J. Wagner, and M. E. Wyman*

I. INTRODUCTION

In Part I of this paper a measurement of the cross section for the reaction $\nu_-(p^+,n^o)\beta^+$ for antineutrinos from fission fragments is described. In order to predict the average cross section for this reaction, one needs to know the energy spectrum.

A measurement of the electron (beta) energy spectrum from fission, enables a determination of the end point distribution for the beta emitters involved. Since this is also the end point distribution for the antineutrino spectra, one can calculate the required antineutrino spectrum. Muehlhause and Oleksa[1] made such a measurement but their results did not permit an unambiguous interpretation of the cross section in terms of the two-component or four-component theory of the antineutrino.

In the present experiment (Fig. 1) a single plastic scintillator was used as the electron spectrometer. This type of detector has a low gamma sensitivity with nearly 100 percent efficiency for electron detection. A gas flow proportional counter placed between the fission source and the scintillator was used as a transmission counter to signal the passage of an electron through it into the scintillator. Using this system for gating a pulse height analyzer, the number of events subjected to pulse height analysis was about 1/4 the total scintillator counts. A fission counter was used as the source of fission electrons in order to determine the number of fissions involved in the measurement. This scintillation spectrometer with its known geometry and a suitable energy calibration was used to measure the number of electrons per fission as a function of energy from 1.5 to 8 Mev.

* University of California, Los Alamos Scientific Laboratory, Los Alamos, New Mexico.

II. EXPERIMENTAL TECHNIQUES

The electron detector (Fig. 1) was a right circular cylinder of Plastifluor B,[2] 1-1/2 inches long and 1-1/2 inches in diameter, cemented to a Dumont 6292 photomultiplier.

The fission beta source was located on the axis of the scintillator cylinder, and was sufficiently distant so that all detected electrons traveled in essentially parallel paths. The resultant path in the scintillator, except for scattered electrons, was 4 gms/cm^2, which is about the maximum range of an 8 Mev electron.

The 1.0639 Mev gamma ray of Bi^{207} which converts in both the K and L shells to give an effective electron line of .991 Mev (for the resolution of this system) was adopted as a convenient calibration standard (Fig. 3). An aluminum absorption measurement, using other conversion lines of Bi^{207} (E_γ = .570 Mev) and Cs^{137} (E_γ = .660 Mev) indicated an energy loss of .043 Mev at the .991 line due to the materials present between the source and the detector. The energy scale was checked within 1 percent at 2.526 Mev using the Tl^{208}(Th C'') line. A measurement of the end points of the beta spectra of F^{20} and Al^{28} agreed with the well known values of 5.41 and 2.87 Mev, respectively (maximum uncertainty 2 percent). In the course of the present experiment the Rh^{104} end point was determined as 2.45 Mev.

The resolution (full width at half-maximum) for monoenergetic electrons was 18.5 percent for the 624 kev Cs^{137} line, and 15.3 percent for the 976 kev Bi^{207} line (K-conversion lines only).

The proportional counter of Fig. 1 was made of two parallel subcounters with a square cross section, with .005-inch steel center wires. The common wall between these two subcounters and the two sides in the path of the electrons were .00025-inch aluminized Mylar. This system was chosen because it gave a relatively small spread in pulse heights from monoenergetic electrons of minimum specific ionization, and also gave reasonably small variations in the time of formation of the pulse after the electron had traversed the counter. The counting gas, 97 percent argon and 3 percent ethane, flowed continuously. The electrons traversed 6.9 mg/cm^2 of material in going through the counter. The most probable pulse size produced by a 991 kev electron was 4.2 kev.

The pulses from the photomultiplier were amplified by both a relatively slow (.3 μsec rise time) linear amplifier, and a fast (.1 μsec rise time) amplifier (Fig. 2). The signal from the fast amplifier, together with that from the transmission counter, were fed to a coincidence circuit, the output of which gated a 100-channel analyzer. The signal from the slow amplifier was analyzed in the 100-channel pulse height analyzer. The widths of the pulses in the coincidence circuit (1 μsec total) and the width of the gating signal to the analyzer (4 μsec) were narrow enough so that, with the counting rates employed, not more than .1 percent of the analyzed counts could have been accidental.

Studies made with a pulser on the pulse widths and delays of the two channels of the coincidence circuit proved that the coincidence and gating system was 100 percent efficient. An additional empirical check on the entire

system was made by comparing the singles counting rate in the scintillator with the number of analyzed counts for a pure beta emitting source. This measurement gave an efficiency greater than 95 percent.

The purpose of the lead shield shown in Fig. 1 was to reduce the backgrounds caused by the reactor (Omega West Reactor at Los Alamos Scientific Laboratory). The number of electrons from the source which might be scattered into the scintillator by the lead was reduced by the polyethylene ring system. The scintillator itself defined the solid angle for detection. In order to minimize the energy loss of the electron before entering the scintillator, the lead collimator and its 5-inch diameter aluminum extension were capped with .00025-inch Mylar, and the chamber thus formed was filled with helium.

Concern about the effect of the shield system on the fission electron spectrum led to a measurement both with and without the shield. The electron spectra in the two cases were almost identical. Similar measurements with allowed beta spectra showed some distortion, but the indications are that the fission spectrum in the energy range from about 1 to 8 Mev is distorted very little.

For a point source, the background could be obtained by absorbing the electrons in a conical shadow shield placed at the appropriate point between the source and detector. Such a shadow cone would remove only the primary electrons, and would allow all scattered electrons and other counted radiation to be properly subtracted from the gross counting rate. A finite source does not permit this, and a shadow cone placed at even the optimum position will unfortunately remove some of the electrons which should properly be considered background. For the present measurements, a 3/4-inch thick graphite shadow shield was inserted as shown in Fig. 1, and the resulting counts were subtracted as background. This would leave a net count which tends to be too large. On the other hand, without the shadow shield, some electrons which start from the source towards the scintillator will be scattered out by gas and windows before reaching it. This will give too low a counting rate. Indications are (from a calibrated Bi^{207} source) that neither of these two effects, which tend to compensate, is greater than 10 percent.

In order to compute the number of betas per fission from the geometry of the system, it was necessary to know the number of fissions. This was accomplished by making the fissionable material the collecting electrode of a fission counter (Fig. 1). None of the fission fragments produced in the thicker foil produced a count in this chamber, so the fission source strength was obtained by multiplying the fission counting rate by the accurately known relative amounts of U^{235} on the two foils. The reactor operating at 800 KW produced about 10^6 slow neutrons per cm^2/sec on the foil. The uncertainty in the source strength is not more than 2 percent.

Additional measurements were made of the increase with time of the number of betas per fission above 1 Mev. After the fission foil had been irradiated for about an hour, this quantity reached a value which is within 3 percent of the value at the end of a 6-hour irradiation. The present data were started after the source had been under irradiation for 1-1/2 hours.

III. CORRECTIONS

After a 2 percent counting rate correction and background subtraction were made the spectrum was raised 0.063 Mev to compensate for the energy degradation by material between the beta emitting fission fragment and the plastic detector.

If the resolution function of the system (its response to monoenergetic radiation) is known, the correction for a continuous spectrum is straightforward.[3] Since monoenergetic electrons in the region of 1.5 to 8 Mev were not available, the resolution function could not be measured. The probable form of this function must be considered in order to estimate the effect on the final result.

An electron, stopped in a scintillator, produces a finite number of photons. The statistics of this process give a predictable gaussian resolution function. However, some of the electrons incident on a scintillator do not deposit all their energy in it. Some electron energy is lost to bremsstrahlung, the photons escaping from the scintillator. The total energy going into bremsstrahlung for a plastic of this type is less than 3 percent in the important energy region of the spectrum (between 2.5 and 5 Mev). Some of the electrons entering the scintillator are scattered back out the front surface without depositing their full energy. The backscattering from this scintillator material has been observed to be 4 percent for the beta spectrum of Yt^{90} which has an end point energy of 2.18 Mev.[4] The fraction of electrons backscattered at higher electron energies is assumed not to increase markedly. The effect of electrons which scatter out the sides of the scintillator was studied for the fission beta spectrum. For the data taken with the 1-1/2 inch scintillator, the scintillator itself determined the aperture of the system and should exhibit a maximum edge effect. With a larger scintillator (2-1/2 inches diameter by 3 inches thick) the shield acted as a somewhat inefficient collimator with at least half the scintillator area shielded. The spectral shapes as seen by the two dissimilar systems were identical but the larger scintillator gives about 5 percent more betas per fission at any energy. This sets an upper limit on the number of electrons scattered out the sides of the 1-1/2 inch scintillator, since the uncertainty in the geometry for the larger system could account for the entire difference. This also demonstrates that the small scintillator is thick enough to detect the high energy end of the spectrum.

Hence the resolution function is the sum of two components. The first is the gaussian resulting from about 90 percent of the electrons which deposit their full energy in the scintillator. Its effect on the true spectrum, a relatively small displacement, upward in energy, has been computed to be 3 kev at 1 Mev increasing to 48 kev at 8 Mev.

The form of the other component, corresponding to the remaining 10 percent of the electrons, is unknown, except that it will appear as a "tail" on the low energy side of the gaussian. Various experimentalists have found that the shape of the "tail" may range from triangular through exponential to rectangular. A rectangular tail extending to zero energy has the greatest effect on the spectrum. In this case, the electrons in the "tail" would not contribute

perceptably to the presently observed spectrum above 2 Mev. The observed spectrum would be too low by the full 10 percent. At 1 Mev the correction would be about 7 percent. Only somewhere below .5 Mev would the curve rise above the true value. It should be noted that the Al^{28} spectrum of Fig. 3 requires a correction equivalent to about half that considered above for agreement with the theoretical shape.

IV. RESULTS

The distribution of scintillator pulse heights for the electrons emitted from fission fragments is shown in Fig. 4. The background obtained with a 3/4 inch thickness of graphite as a shadow absorber is shown on the same figure. During the course of experimentation the fission beta spectrum was measured with different solid angles, with and without shielding, and with different detectors. In each case the shape of the spectrum above 1 Mev was invariant (within statistics). The data presented here are from the experimental system as described and represents only one of the many measurements. The data corrected as indicated in Section III and transformed to betas per fission per Mev is shown in Fig. 5.

$$Y(E_\beta) = 3.88 \exp \left[-.575\, E_\beta - .055\, E_\beta^2 \right] \tag{1}$$

(E_β is the electron kinetic energy in Mev) is an analytic function which fits the experimental data in the important energy region. It is represented by the solid line on Fig. 5. Using this analytic expression, a beta spectra end point distribution was calculated on an IBM 704 electronic computing machine for emitters with Z = 32 and also for Z = 60 (Fig. 6). From these end point distributions the neutrino spectra were calculated. For the details of this calculation see Appendix II. These spectra are shown in Fig. 5 along with the beta spectrum.

The antineutrino absorption cross section per fission is then given by

$$N\bar{\sigma} = \int_{1.8\ \text{Mev}}^{\infty} \sigma(E_{\nu_-})\ \rho(E_{\nu_-})\, dE_{\nu_-} \tag{2}$$

where $\sigma(E_{\nu_-})$ = the theoretically predicted cross section as a function of the antineutrino energy (for details see Appendix I).

$\rho(E_{\nu_-})$ = the number of antineutrinos per fission per Mev at energy E_{ν_-}.

The number of antineutrinos per fission above the threshold for the reaction is

$$N = \int_{1.8\ \text{Mev}}^{\infty} \rho(E_{\nu_-})\, dE_{\nu_-}. \tag{3}$$

The average absorption cross section per antineutrino above the threshold for the reaction is

$$\bar{\sigma} = \int_{1.8\ \text{Mev}}^{\infty} \sigma(E_{\nu_-})\ \rho(E_{\nu_-})dE_{\nu_-} \Big/ \int_{1.8\ \text{Mev}}^{\infty} \rho(E_{\nu_-})dE_{\nu_-}. \qquad (4)$$

Using the values of $\rho(E_{\nu_-})$ from Fig. 5, $N\bar{\sigma}$, N and $\bar{\sigma}$ were calculated for Z = 32 and 60. The results are shown in Table I.

TABLE I. Summary of Results

Z	$N\bar{\sigma}$	N (above 1.8 Mev)	$\bar{\sigma}$
32	5.2×10^{-43} cm^2/fission	1.85 ν_-/fission	2.8×10^{-43} cm^2/ ν_-
60	6.2×10^{-43}	2.02	3.1×10^{-43}

As the best value of $N\bar{\sigma}$ we quote $N\bar{\sigma} = 5.7 \times 10^{-43}$ cm^2/fission.

V. RELIABILITY

It is difficult to determine the errors in an experiment of this type where absolute values of quantities are required. The following is a list of sources of error and an estimate of their effect on the final cross section prediction: (a) total fissions, ±2 percent; (b) energy calibration, ±1 percent; (c) background, ±8 percent; (d) uncertainty in applying corrections for energy loss and symmetrical part of resolution, ±1 percent; (e) analytic fit to data, ±2 percent; (f) uncertainty in the theoretical cross section for monoenergetic antineutrinos caused by the uncertainty in the measured neutron half-life, ±13 percent; (g) distribution of the Z's of the fission product beta emitters, ±5 percent (see Table I).

Considering only the sources of error indicated above, a maximum uncertainty of ±25 percent could be assigned. It seems reasonable to believe that the correct answer should fall within ±15 percent.

There is an uncertainty which is not included in the above. It was not possible to correct our results for the asymmetric resolution of the scintillator and the departure from secular equilibrium of the fission beta spectrum. The correction would be such as to increase the cross section per fission by an amount which should not exceed 10 percent.

Hence our result of 5.7×10^{-43} cm^2/fission could be raised as high as 6.3×10^{-43} cm^2 and should have a reliability of ±1 $\times 10^{-43}$ cm^2/fission. A reasonable result would be $6.0 \pm 1 \times 10^{-43}$ cm^2/fission.

On the same basis, the value of the antineutrinos per fission above 1.8 Mev is 2.0 ± .2 ν_-/fission.

The cross section per antineutrino above 1.8 Mev would be $3.1 \pm .4 \times 10^{-43}$ cm^2/ ν_-.

VI. ACKNOWLEDGMENT

We wish to thank Mr. E. H. Kinney for assistance with the numerical computations, members of the Physics Division reactor group for helpful discussions, and to Mr. J. G. Povelites and Dr. E. H. VanKooten for the preparation and weighing of the fission foils.

APPENDIX I

The predicted cross section for $\nu_-(p^+,n^o)\beta^+$

For a monoenergetic ν_- as derived for the four-component neutrino by Konopinski (private communication - 1953), and others,

$$\sigma(E_{\nu_-}) = \frac{G^2}{2\pi}\left(\frac{\hbar}{mc}\right)^2\left[\frac{E_{\nu_-}}{mc^2} - \frac{M_n - M_p}{m}\right]\sqrt{\left[\frac{E_{\nu_-}}{mc^2} - \frac{M_n - M_p}{m}\right]^2 - 1} \qquad (5)$$

$M_n - M_p$ = neutron, proton mass difference and mc^2 is the rest energy of the electron.

$$\left[\frac{M_n - M_p}{mc^2}\right]c^2 = \frac{1.293}{0.511} = 2.530 \text{ and threshold is at } 2.530 + 1 = 3.530$$

$$= 3.530 \times 0.511 = 1.804 \text{ Mev.}$$

According to DuMond and Cohen,[5] $h/mc = 2.426 \times 10^{-10}$ cm, or

$$\left(\frac{\hbar}{mc}\right)^2 = \left(\frac{2.426 \times 10^{-10}}{2\pi}\right)^2 = 1.491 \times 10^{-21} \text{ cm}^2.$$

As pointed out by Lee and Yang, and others,[6] the formula can be generalized to include the two-component neutrino by addition of a factor P which is unity in the four-component theory and 2 for the two-component neutrino. This result follows from the restriction in the two-component theory of final states in the neutron decay.

$$\sigma(E_{\nu_-}) = \frac{P\,G^2}{2\pi} \times 1.491 \times 10^{-21}\,(E_{\nu_-} - 2.530)\sqrt{(E_{\nu_-} - 2.530)^2 - 1} \qquad (6)$$

where: E_{ν_-} = antineutrino energy in mc^2 units

G^2 = appropriate β coupling constant

P = parity factor = 1, four-component ν_-

= 2, two-component ν_-.

We will evaluate $\left(\frac{\hbar}{mc}\right)^2 \frac{G^2}{2\pi} = \alpha$ from the properties of neutron decay.

If we redefine G^2 in terms customarily used in β decay theory,

$$G^2/2\pi = g^2/2\pi \times m^2/\hbar^4.$$

Then $$\frac{1}{\tau_n} = g^2 \frac{m^5 c^4 F(\eta_o)}{2\pi^3 \hbar^7}$$

and $$\alpha = \frac{1}{2\pi\,\tau_n} \times \frac{2\pi^3 \hbar^7 c}{(mc)^5 F(\eta_o)} \times \frac{m^2}{\hbar^4} = \frac{\pi^2}{c} \frac{\hbar^3}{(mc)^3} \frac{1}{\tau_n F(\eta_o)}$$

where $\tau_n = \tau_{1/2}/0.693 = (12 \pm 1.5/0.693) \times 60 = 1040 \pm 130$ sec and[7] the Fermi function $F(\eta_o) = F(P_{max}/mc) = F(2.324) = 1.633$.

The β^- spectrum from neutron decay measured by J. M. Robson[8] is consistent with an allowed shape having an end point of 782 kev.

Finally, $$\alpha = \frac{\pi^2}{c} \left(\frac{\hbar}{mc}\right)^3 \frac{1}{\tau_n F(\eta_o)}$$

$$= \frac{\pi^2}{3 \times 10^{10}} \left(\frac{2.426 \times 10^{-10}}{2\pi}\right)^3 \times \frac{1}{1040 \pm 130} \times \frac{1}{1.633}$$

$$\alpha = 1.12 \pm 0.14 \times 10^{-44}\ \text{cm}^2,$$

so that the desired cross section for a monoenergetic antineutrino is

$$\sigma(E_{\nu_-}) = (1.12 \pm 0.14) \times 10^{-44} (E_{\nu_-} - 2.53) \left[\sqrt{(E_{\nu_-} - 2.53)^2 - 1}\right] \times P \qquad (7)$$

where σ in cm^2 and E_{ν_-} is in mc^2 units.

APPENDIX II

The cross section for fission fragment antineutrinos

The β^- spectrum from fission fragments differs from the associated ν_- spectrum because of the finite mass of the electron and the spectral distortion due to electrostatic attraction between the electron and nucleus. Since, given an end point and coulomb factor, both the β^- and ν_- are determined, the problem is viewed as one of determining the end point distribution, considering coulomb effects. However, we do not as yet know the details of the short lived fission product chains and hence it is not possible to accurately predict these effects. Consequently, we adopt a procedure which enables us to bracket the expected cross section. We assume that the observed β^- spectrum results from the superposition of a continuous distribution of β^- emitters, each one having an allowed shape but all with the same nuclear charge Z. Two extreme values of Z (Z = 60,32) are assumed so as to place upper and lower limits on the coulomb distortion of the β^-, and hence the ν_- spectrum. The end point distribution is then determined by solving the appropriate integral equation and the cross section of Appendix I is integrated over the resulting ν_- spectrum.

The experimentally determined β^- spectrum $Y(E_\beta)$ is related to the end point distribution $n(E,Z)$ by the integral equation

$$Y(E_\beta) = \int_{E = E_\beta}^{\infty} n(E,Z)B(E,Z)\, f\,(E,E_\beta,Z)dE \tag{8}$$

where $B(E,Z)$ is the normalization function for the allowed β^- spectrum $f(E,E_\beta,Z)$

$$B^{-1}(E,Z) = \int_{E_\beta = 1}^{\infty} f(E,E_\beta,Z)dE_\beta \tag{9}$$

and E_β is the total beta energy, including the rest energy. In general

$$f(E,E_\beta,Z) = E_\beta^2\,(E - E_\beta)^2\, G(Z,P_\beta) \tag{10}$$

where
$$G(Z,P_\beta) = (P_\beta/E_\beta)\, F(Z,P_\beta). \tag{11}$$

F is the Fermi coulomb function,[9] and P_β is the electron momentum.
For $Z = 32$, $G(32,P_\beta) = a$, which is constant to ± 6 percent and

$$f(32,E_\beta,E) = E_\beta^2(E - E_\beta)^2\, a. \tag{12}$$

For $Z = 60$, $G(60,P_\beta)$ is represented to within ± 2 percent by the function

$$G(E_\beta) = be^{-0.16\ \sqrt{E_\beta - 1}} \tag{13}$$

over the range $E_\beta = 1 \longrightarrow 15\ mc^2$.

We now solve, for $n(E,Z)$, assuming Z independent of E. Rewriting (8),

$$M = Y/E^2G = \int_{E = E_\beta}^{\infty} m(E,Z)(E - E_\beta)^2 dE \tag{14}$$

where
$$m(E,Z) = n(E,Z)\, B(E,Z). \tag{15}$$

Differentiating (14) with respect to E_β three times, we find:

$$m(E_\beta,Z) = -1/2\ \frac{d^3\, M(E_\beta)}{dE_\beta^3} \tag{16}$$

and the end point distribution is obtained from (15) and (16).

The fission fragment ν_- spectrum, $\rho(E,Z)$ is then given by adding the spectra having the calculated end point distribution, $n(E,Z)$

$$\rho(E,Z) = \int_{E = E_{\nu_-} + 1}^{\infty} n(E,Z)B(E,Z)\, f'(E_{\nu_-},E,Z)dE \tag{17}$$

For $Z = 32,\ f' = (E - E_{\nu_-})^2 E_{\nu_-}^2,$

$$Z = 60,\ f' = (E - E_{\nu_-})^2 E_{\nu_-}^2 \exp\left[-.16\sqrt{E - E_{\nu_-} - 1}\right] \tag{18}$$

The average cross section per fission, $(N\bar{\sigma})$, for the fission ν_- spectrum is then given by

$$N\bar{\sigma}(Z) = \int_{E_{\nu_-} = 3.53}^{\infty} \sigma(E_{\nu_-})\ \rho(E_{\nu_-}, Z)\, dE_{\nu_-} \tag{19}$$

The number, N, of antineutrinos above a certain energy is

$$N = \int_{E_{\nu_-}}^{\infty} \rho(E_{\nu_-}, Z)\, dE_{\nu_-} \tag{20}$$

REFERENCES

1. Muehlhause, C. O., and Oleksa, S., Antineutrino Flux from a Reactor, Phys. Rev. 105:1332-4, (1957).

2. Pilot Chemicals, Inc., 47 Felton Street, Waltham 54, Massachusetts.

3. Owen, G. E., and Primakoff, H., Relation between Apparent Shapes of Monoenergetic Conversion Lines and of Continuous β-Spectra in a Magnetic Spectrometer, Phys. Rev. 74:1406-12, (1948); R.S.I. 21:447-50, (1950) Part II.

4. Muller, D. C., Interaction of Beta Particles with Organic Compounds, Analyt. Chem. 29:975-8, (1957).

5. DuMond, J. W. M., and Cohen, E. R., Least-Squares Adjusted Values of the Atomic Constants as of December, 1950, Phys. Rev. 82:555-6, (1951).

6. Lee, T. D., and Yang, C. N., Parity Nonconservation and a Two-Component Theory of the Neutrino, Phys. Rev. 105:1671-5, (1957).

7. Spivak, P. E., Sosnosky, A. N., Prokofiev, A. Y., and Sokoloff, V. S., Investigation of Neutron Beta Decay, Geneva Conference Report Vol. 2: 33-8, (1955).

8. Robson, J. M., The Radioactive Decay of the Neutron, Phys. Rev. 83:349-58, (1951).

9. These functions are given by M. E. Rose in the appendix to Chapter IX in Beta- and Gamma-Ray Spectroscopy, edited by K. Siegbahn, Interscience Publishers, Inc., New York, (1955).

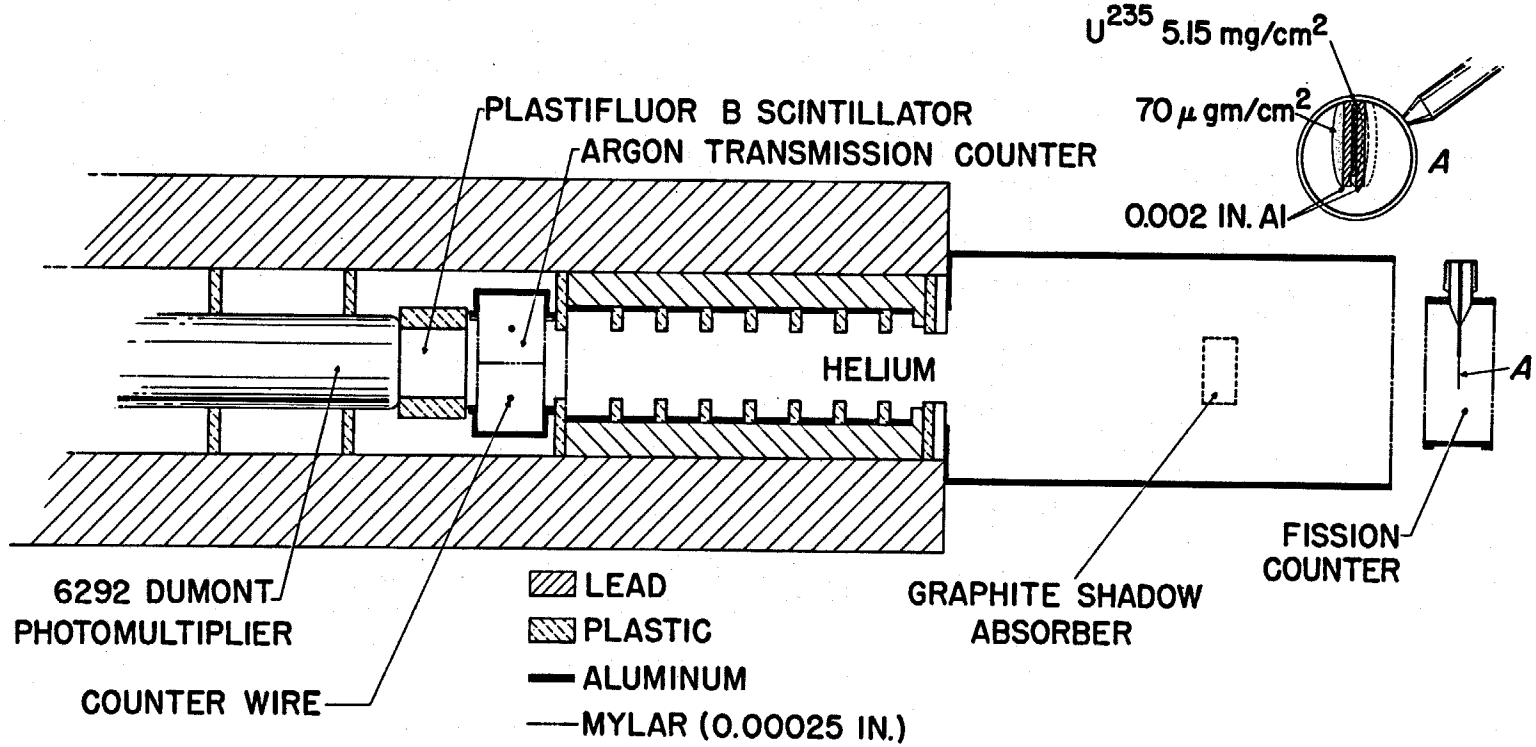

Fig. 1. The experimental arrangement.

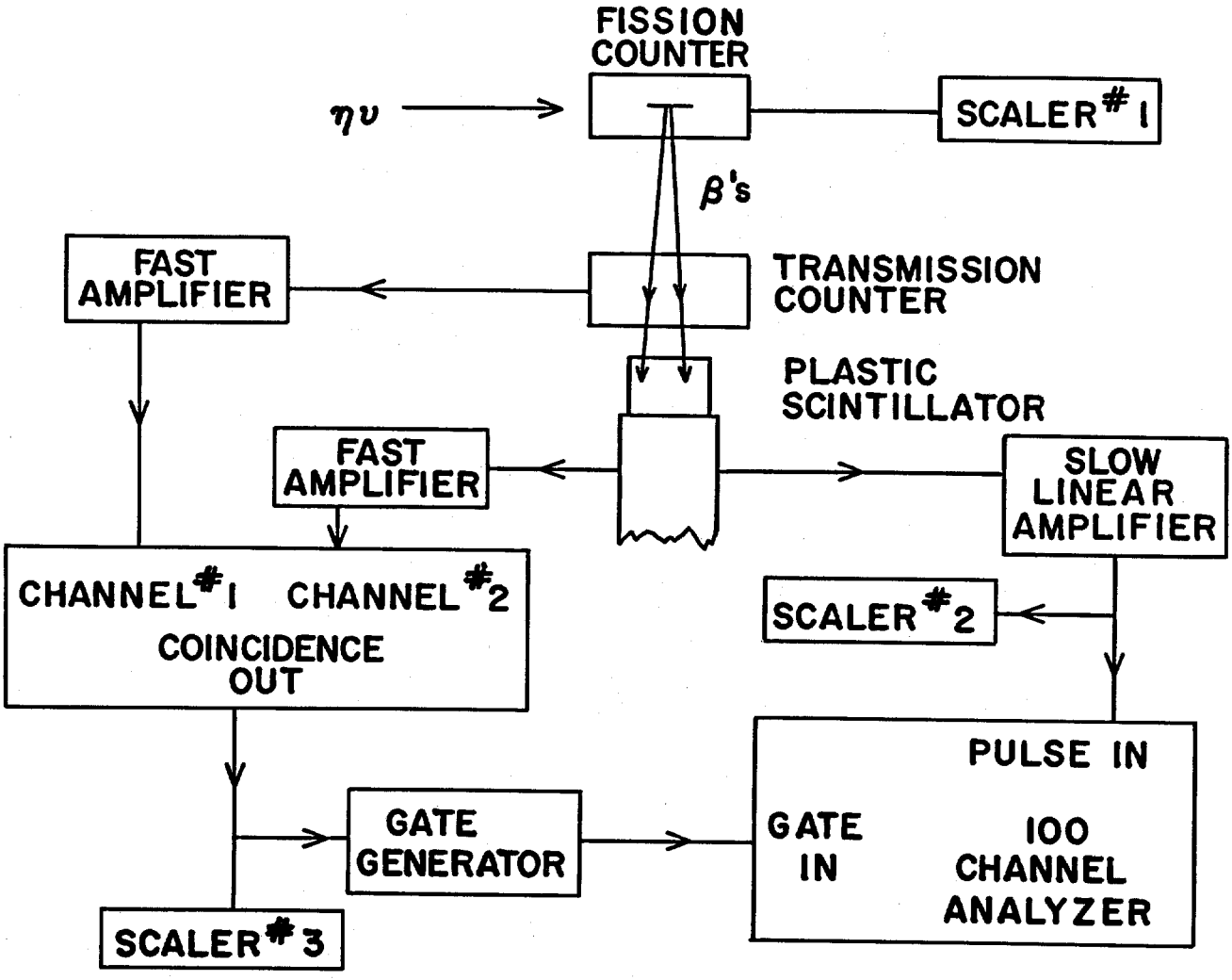

Fig. 2. Block diagram of electronic circuits.

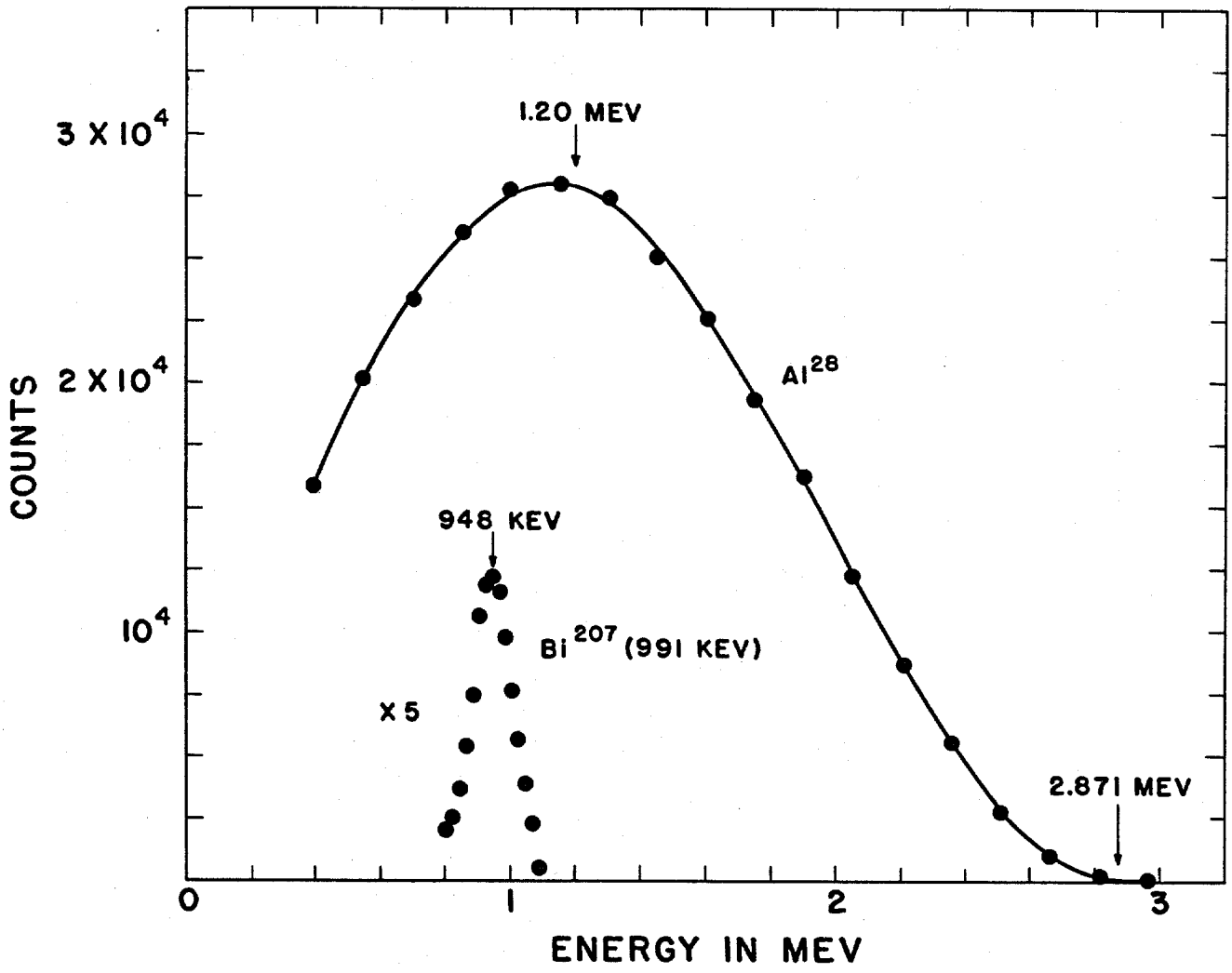

Fig. 3. Al^{28} beta spectrum and Bi^{207} calibration.

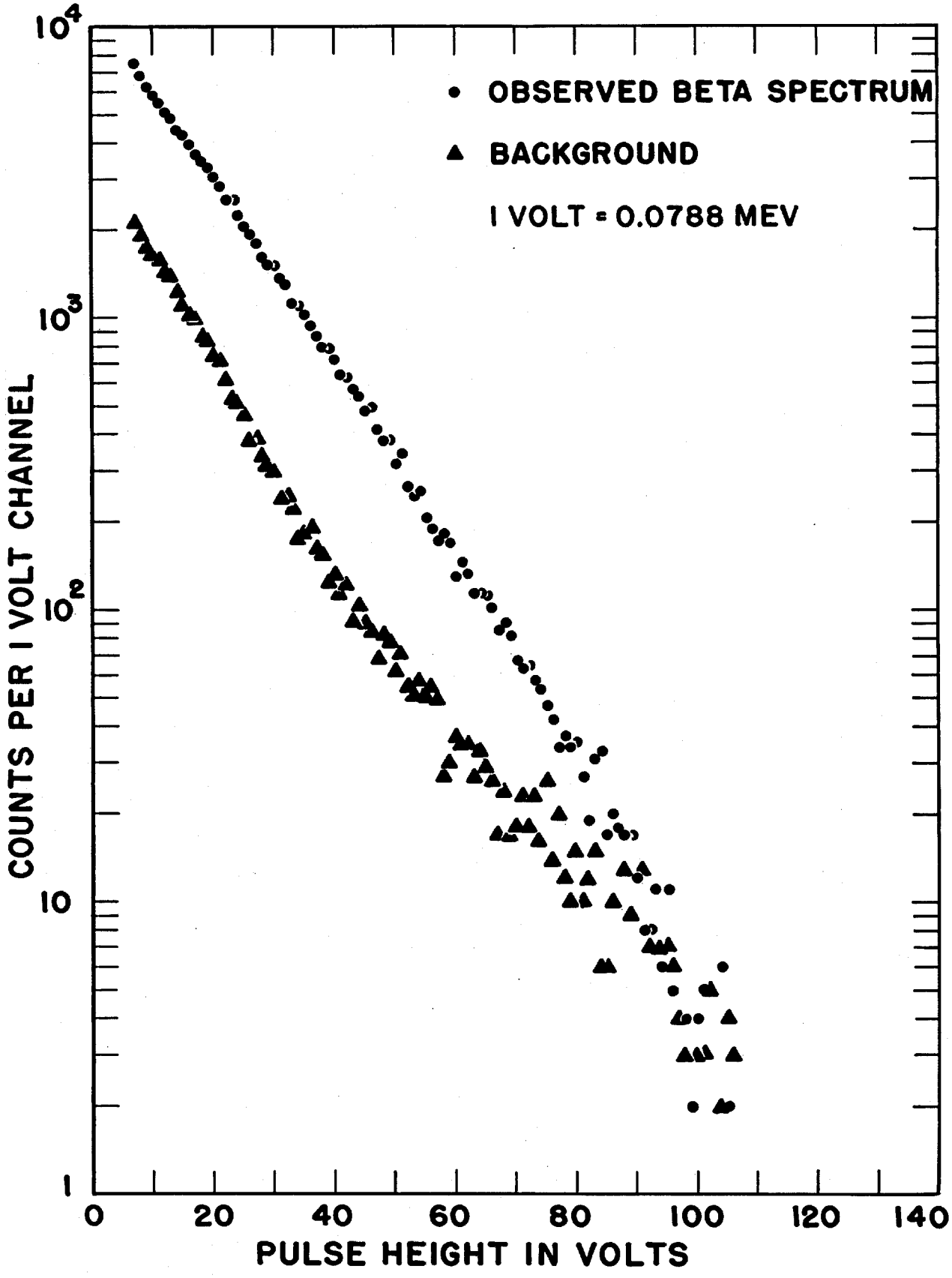

Fig. 4. Fission beta data as taken from the 100-channel analyzer.

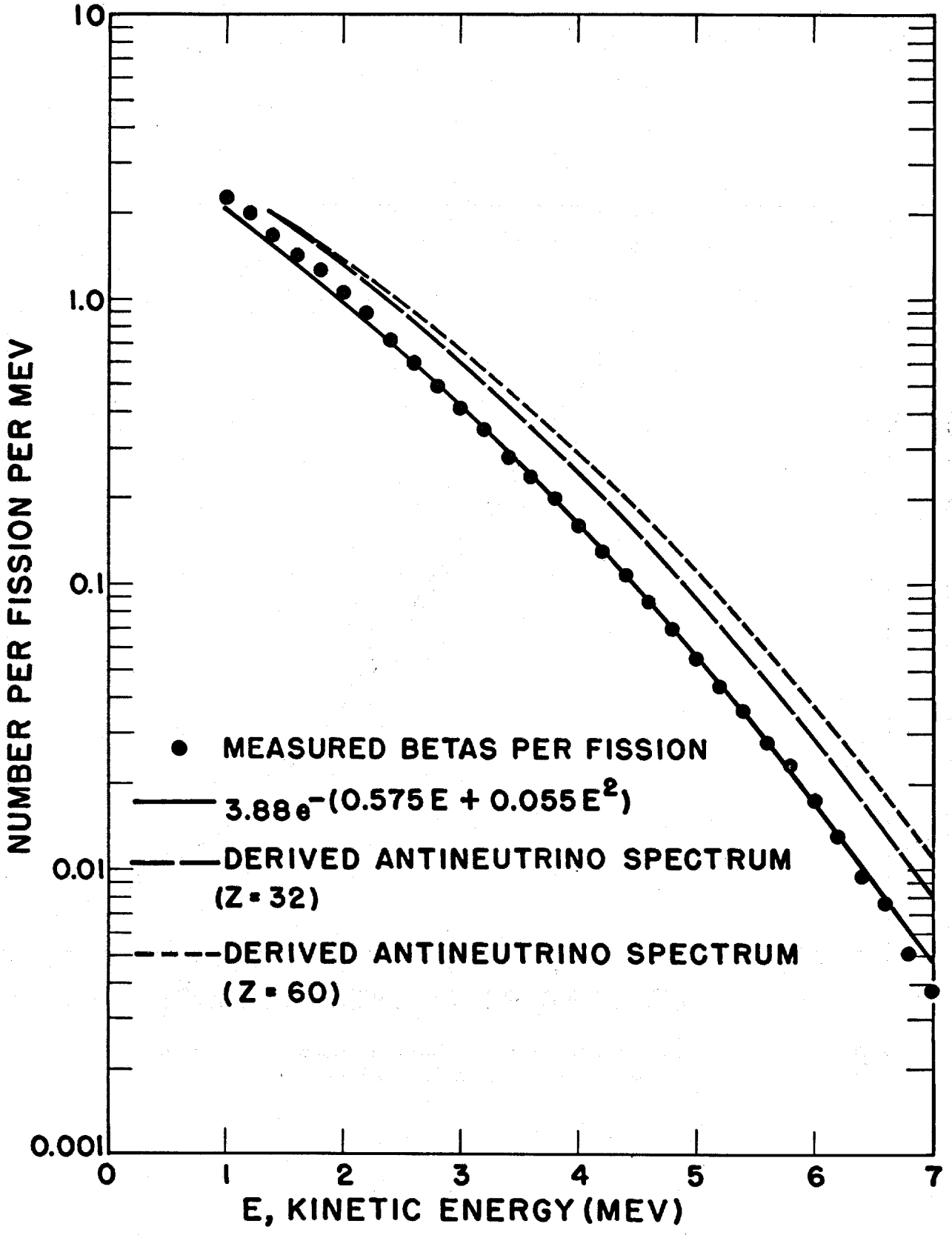

Fig. 5. Corrected results, the empirical fit to the data, and the derived antineutrino spectra.

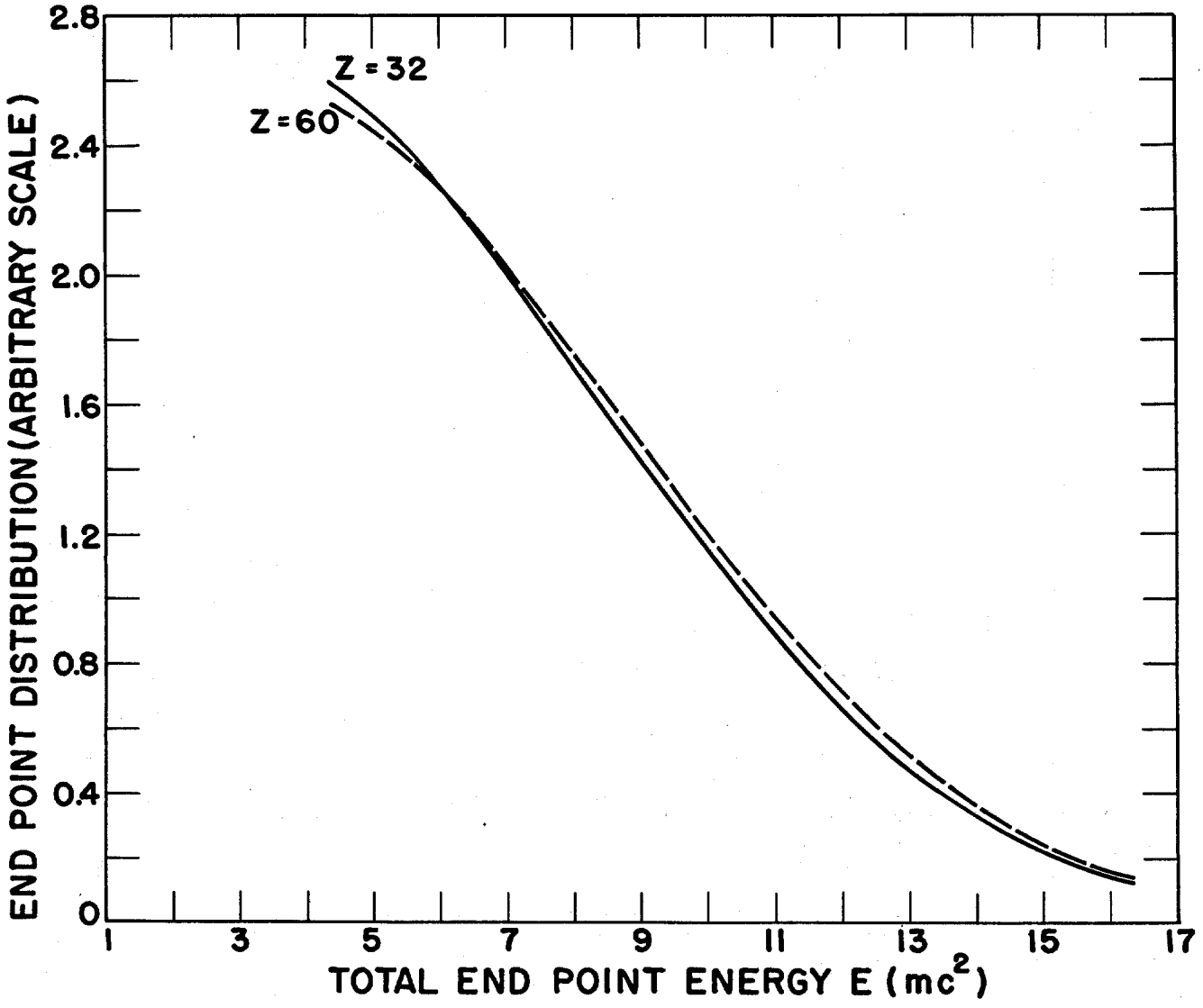

Fig. 6. The end point distribution, assuming allowed shapes for the individual spectra.

THE FREE ANTINEUTRINO ABSORPTION CROSS SECTION

INTERPRETATION OF RESULTS

The measured cross section for the reaction $\bar{\nu}_-(p^+,n^0)\beta^+$ for antineutrinos from fission fragments is $\bar{\sigma}N = (6.7 \pm 2.4) \times 10^{-43}$ cm^2/fission. This result is in agreement with theoretical expectation,[1] $\bar{\sigma}N = 6.0 \pm 1 \times 10^{-43}$ cm^2/fission, based on the measured fission β^- spectrum, the two-component theory of the neutrino, the principle of microscopic reversibility, and the measured characteristics of neutron decay. A more precise measurement of the absorption cross section is of interest in order to sharpen our conclusions and indeed such increased precision is now feasible.

[1] An independent prediction made by King and Perkins from a consideration of the details of the fission chains gives for the two-component neutrino theory the result $\bar{\sigma}N = 9 \times 10^{-43}$ cm^2.

King, R. W. and Perkins, J. F., Inverse Beta Decay and the Two-Component Neutrino (to be submitted to the Physical Review). We wish to thank Dr. King for this information in advance of publication.